

Electron microphysics at plasma-solid interfaces

F. X. Bronold, K. Rasek and H. Fehske

Institut für Physik, Universität Greifswald, 17489 Greifswald, Germany

(Dated: November 20, 2021)

The most fundamental response of a solid to a plasma and vice versa is electric. An electric double layer forms with a solid-bound electron-rich region—the wall charge—and a plasma-bound electron-depleted region—the plasma sheath. But it is only the plasma sheath which has been studied extensively ever since the beginning of plasma physics. The wall charge received much less attention. Especially little is known about the in-operando electronic structure of plasma-facing solids and how it affects the spatio-temporal scales of the wall charge. The purpose of this perspective is to encourage investigations of this terra incognita by techniques of modern surface physics. Using our own theoretical explorations of the electron microphysics at plasma-solid interfaces and a proposal for measuring the wall charge by infrared reflectivity to couch the discussion, we hope to put together enough convincing reasons for getting such efforts started. They would open up—at the intersection of plasma and surface physics—a new arena for applied as well as fundamental research.

I. INTRODUCTION

Low-temperature plasmas, ionized gases with electron and ion temperatures of at most a few tens of an electron volt, are technologically extremely successful. They are used in devices for particle detection, lighting, welding, sterilization, pollutants management, and ozone production, as well as in various sorts of materials modifications and syntheses. In all these applications it is either the chemistry inside the bulk plasma or the structural and chemical aspects of plasma-solid interaction which are commercially exploited. A number of roadmaps have been laid out suggesting how plasma physics should evolve to make it economically even more valuable than it already is [1–3]. In this perspective we will not compete with them. Instead we will focus on another aspect of plasma-solid interaction: the electric response of the solid to the plasma and vice versa leading to an electric double layer at the interface. Particularly the solid-bound part of the double layer has been largely overlooked. Including it into the physical investigations, and considering it as part of the in-operando modification of the electronic properties of a plasma-facing solid, new vistas for fundamental as well as applied research at the intersection of plasma and solid state physics may open up.

Double layers are ubiquitous in nature. They arise at interfaces due to charge separation. Perhaps the most prominent double layer occurs at the basic building block of a battery, the electrolyte-metal interface [4, 5]. But also the Schottky contact [6], the semiconductor-metal interface omnipresent in solid state electronics, gives rise to a double layer. In fact, there are many more interfaces and hence double layers of technological relevance. Of particular current interest are, for instance, interfaces of large energy gap tertiary oxides [7, 8]. The buried electron gases forming there and being the objects of study are the negative legs of electric double layers. In plasma physical settings, double layers arise when two gaseous plasmas face each other [9, 10] or when a plasma faces a solid.

The double layer developing at the plasma-solid in-

terface, with a solid-bound electron-rich and a plasma-bound electron-depleted region, is the object of this perspective. It is known since the very beginning of plasma physics [11]. In the simplest case, it arises because electrons outrunning the ions are deposited more efficiently into or onto the solid, depending on its electronic structure, than they are extracted from it by the neutralization of the ions. The plasma-bound part of the double layer—the plasma sheath—has been thoroughly investigated [12, 13], most notably, its matching with the bulk plasma [14–17] and its structural changes due either to negative ions [18] or the emission of electrons from the wall [19–21]. The structure of the sheath in front of biased electrodes received recently also substantial attention [22]. But little is known about the solid-bound part—the wall charge. No systematic investigations exist about its material dependence or its depth profile perpendicular to the interface. The magnitude [23–25] of the wall charge and also its lateral distribution [26, 27] can be measured by particularly designed setups, but the electronic states hosting it are unknown.

From our point of view, the electron microphysics at plasma-solid interfaces, comprising electron deposition and extraction to and from the solid, the build-up of the double layer, and—most importantly—the in-operando electronic structure of the plasma-facing solid, is an unexplored territory. Very often the solid is only treated as an electron reservoir, characterized by a geometric boundary and probabilities for electron extraction and deposition. As long as the probabilities are simply adjustable parameters, the effect of the wall on the properties of Hall thrusters [28], radio-frequency discharges [29], dusty plasmas [30, 31], and dielectric barrier discharges [32, 33], to name only a few of the many technologically relevant plasma applications, can be studied without going into the details of the wall’s electron microphysics. It is then also sufficient to model the wall charge as an idealized infinitely thin surface charge. However, if one wants to have control over the surface parameters, or if one wants to understand how the wall charge affects the functionality of the discharges, one has to explore the electronic

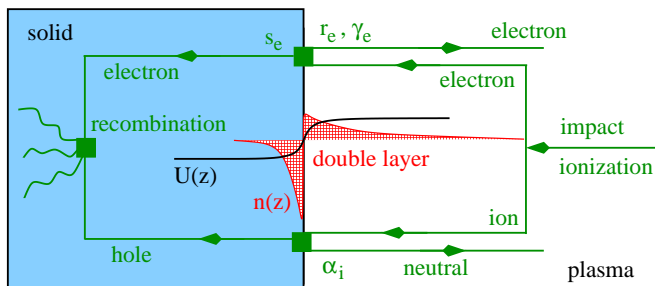


FIG. 1. Electrons and ions generated inside a plasma by impact ionization hit a plasma-facing solid. Usually probabilities for electron sticking (s_e), reflection (r_e), secondary emission (γ_e), and ion neutralization (α_i) are used to characterize the effect the solid has electronically on the plasma. What the holes and electrons injected into the solid and making up the negative leg of an electric double layer, whose positive one is the plasma sheath, are doing is ignored. We argue in this perspective that the electron microphysics at the interface, comprising the charge dynamics on both sides of it and the in-operando electronic structure of the plasma-facing solid, should be the subject of physical inquiry.

processes inside the plasma-embracing solid in detail.

The memory effect in dielectric barrier discharges [34, 35], for instance, that is, the phenomenon that the electric breakdown preferentially occurs at locations where wall charges from the previous one still reside on or inside the dielectric, depends on the type of electronic states the charges are bound to. On the macroscopic scale, the memory effect has been investigated intensively [36, 37]. What is missing is a microscopic inquiry. With the insights gained from it it would be perhaps possible to manipulate the discharge by a judicious choice of the dielectric material. For the control of catalytic surface reactions, often the technological purpose of this type of discharges, a microscopic understanding of what is going on electronically inside the dielectric would be also rather useful [38, 39]. This statement even holds for ozonizers, perhaps the oldest application of barrier discharges, where optimization procedures for the dielectric stacks are still guided by empiricism.

Miniaturized semiconductor-based microdischarges are another type of discharge, where electronic processes inside the solid play an increasingly important role [40–43]. For future progress, it seems to be essential to treat the charge kinetics inside the plasma and the solid on an equal footing [44–48]. At least it is conceivable to realize by continuing miniaturization situations, where the scales for charge transport and relaxation are comparable for both subsystems. Electrons inside the solid may then be equally hot as the electrons in the plasma, that is, on the order of a few electron volts, which should strongly affect, for instance, the in-operando interface resistance and hence the electronic characteristics of the discharge. Since these devices combine aspects of gaseous and solid state electronics they may be of interest for optoelectronic applications [42]. Assuming materials issues, such

as structural damage due to ion implantation [43], which are a problem at the moment, can be solved, progress will still depend on an holistic approach considering electronic processes inside the solid and the plasma as equally important. Only then will it be possible to tap the full technological potential of this type of microdischarges.

This perspective strongly bats for a systematic study of the electron microphysics at the plasma-solid interface. It asks not only for calculating the probabilities for electron deposition and extraction from microscopic models for the surface but also for the selfconsistent description of the chain of events shown in Fig. 1. A kinetic theory is thus the goal, which tracks the charges created by impact ionization on the gaseous side of the interface to the inside of the solid, where they annihilate to phonons or photons. Essential for both theoretical tasks is a precise knowledge of the in-operando electronic structure of the plasma-facing solid. It is thus necessary to enlarge the experimental toolkit by techniques of modern surface diagnostics [49], which fortunately are no longer limited to vacuum-solid interfaces but cover nowadays also liquid-solid [50–54] and solid-solid interfaces [55–62]. We strongly call for applying these techniques to plasma-solid interfaces. So far, this has been done only occasionally [63–67]. It is the combined theoretical and experimental effort we hope to initiate by this perspective which would provide an unprecedented view of the electronics of the plasma-solid interface. In the long run, we are convinced, this will be the basis for new concepts of solid-bound low-temperature gas discharges.

In the next section we use our own work to exemplify the two basic theoretical aspects of the interface's electron microphysics by, respectively, a calculation of the probability with which an electron is absorbed by a metal at energies low enough to be of relevance for plasma applications and a semiclassical kinetic model for the double layer at a dielectric plasma-solid interface. In addition, we present an experimental scheme for investigating the wall charge by infrared reflection spectroscopy. Exploratory calculations are rather promising and we hope experimentalists put it into work. Having discussed results of our own work, we next plea for in-operando studies of the electronic structure of plasma-facing solids by photoemission and electron spectroscopy. The techniques cannot be applied directly to the interface. We envisage therefore spinning wall and from-the-back arrangements. Albeit expensive, and certainly requiring long term commitment, having them on board would be especially beneficial because they provide the microscopic information most relevant for the electronics of the plasma-solid interface: chemical composition, presence or absence of surface states, and energy barriers due to the profile of the electric potential. In the course of the plea we also indicate materials which we consider to be of interest for fundamental as well as applied research. In a concluding synopsis we finally summarize our main points for quick reference.

II. WORK WE ARE DOING

The pragmatic approach towards the plasma wall is to consider it as an electron reservoir. Leaving structural damage due to heavy particles aside, the wall is then characterized by a fixed geometric boundary and probabilities for electron sticking (s_e), reflection (r_e) and (secondary) emission (γ_e). The latter may arise due to electron impact or charge-transferring encounters with heavy particles, such as ions or radicals, giving rise to various Auger-type processes. As far as electrons are concerned, impact energies are typically well below 1 keV, making theoretical approaches and techniques developed for the description of electron spectroscopy and microscopy not applicable. In addition, it has been noticed that in this energy range measured data are also sparse [68, 69], triggering hence efforts to calculate [70–73] or to measure some of the probabilities, usually called surface parameters, by beam [74–78] or plasma experiments [79–82].

Beam experiments for measuring γ -coefficients due to ion [77] or electron impact [74, 75, 78] are highly relevant but have the drawback of not being made under plasma operation. Plasma experiments, on the other hand, enable an in-operando determination of electron sticking [79, 80] and γ -coefficients [81, 82]. They depend however on simulations of the gas discharge under the assumption that the coefficient to be determined is the only one unknown. Calculating the coefficients from first principles is also rather challenging. Even the simplest projectile, the electron, gives rise to scattering cascades involving many different collision paths. Ions and radicals, having internal degrees of freedom, lead to even more involved collisions [83, 84].

Our calculations of electron surface parameters are based on semiempirical effective Hamiltonians for the subset of electronic states which are most relevant for the collision process under consideration. The matrix elements of the Hamiltonians can be either determined experimentally or theoretically from first principles. Initially, we applied the semiempirical approach to secondary electron emission due to heavy particles [70, 71] and electron scattering off dielectric surfaces [72, 73]. But later on we also used it for the kinetic modeling of the electric response of a dielectric plasma-solid interface [44, 48]. To identify the kind of information needed about the interface's electronic structure to make the semiempirical approach work, we illustrate in the following the calculational schemes with some new results. The link between our work and the work we hope to initiate is the proposal for measuring the wall charge by infrared reflectivity described at the end of this section. It calls for experimentalists to implement it.

A. Electron absorption by metallic walls

An important surface parameter, controlling the charging of dust particles immersed in a plasma [30, 31], is the

electron sticking coefficient. Its complement, the electron emission yield due to electron impact, plays an important role in Hall thrusters [28] and barrier discharges [32, 33]. Based on the invariant embedding principle for electron scattering off surfaces [85–87], we set up in our previous work [72, 73] a scheme for calculating electron sticking coefficients for dielectric surfaces at energies below the band gap. In this subsection we apply it to a low energy electron scattering off a metallic surface. The intention is to identify the parts of the electronic structure of the metal which should be known as precisely as possible. If they are affected by the plasma, they should be measured in-operando.

An electron hitting a metallic surface enters, after successful transmission through the surface potential, the conduction band. As illustrated in Fig. 2, elastic and inelastic scattering events inside the metal may push the electron back to the interface, where it may traverse the surface potential in the reverse direction to leave the solid again. The probability for coming back to the plasma is thus the result of passing twice through the surface potential and diffuse scattering in between. Notice, only electrons from the plasma with an energy high enough to overcome the wall (sheath) potential U_w have a chance to perform such a cascade. Putting the origin of the energy axis to the potential just outside the solid, we thus have to track only electrons impacting with $E > 0$. That the electron performing the cascade stems from the plasma is irrelevant. The plasma affects the cascade only indirectly through the depth U_0 of the surface potential, which is the sum of the Fermi energy E_F and the work function Φ . Both may depend on the surface's chemical contamination and structural modification by the plasma. Hence, E_F and Φ should be measured in-operando. In case the metal is biased, the situation is essentially the same except that, depending on the polarity of the bias voltage $\pm V_{\text{bias}}$, the wall potential U_w is reduced (positive bias) or increased (negative bias) by the amount eV_{bias} . The material parameters E_F and Φ , however, are unaffected.

To describe the scattering cascades we use the variables and probabilities defined in Fig. 2. The sticking probability $S(E, \xi)$, where E is the energy and ξ the cosine of the angle β with which the primary electron hits the surface with respect to the inwardly directed surface normal is then given by [72, 73]

$$S(E, \xi) = T(E, \xi) - T(E, \xi) \times \int_{\eta_{\min}(E)}^1 d\eta' \int_{E_{\min}(\eta')}^E dE' \rho(E') B(E\eta(\xi)|E'\eta') T(E', \xi(\eta')) , \quad (1)$$

where $\xi = \cos\beta$, $\xi' = |\cos\beta'|$, and $0 < \beta \leq \frac{\pi}{2} < \beta' \leq \pi$. The function $T(E, \xi)$ is the probability for quantum-mechanical transmission through the surface potential and $B(E\eta|E'\eta')$ is the probability for scattering inside the solid from the state (E, η) to the state (E', η') , where $\eta = \cos\theta$ and $\eta' = |\cos\theta'|$ are the direction cosines inside the solid. The upper limit to the energy integral accounts

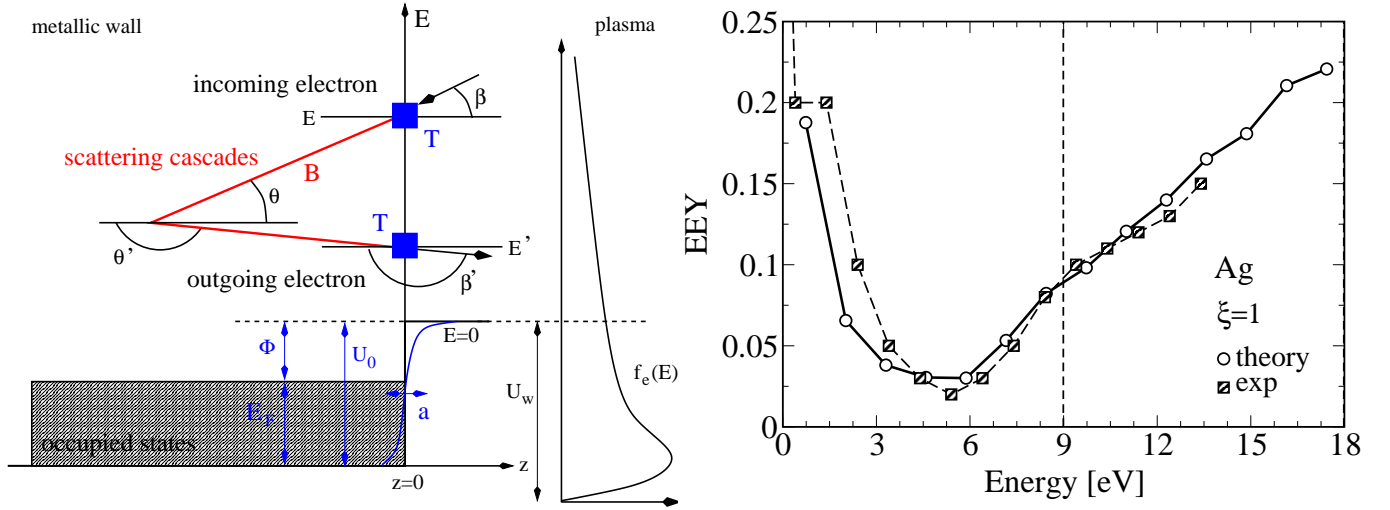


FIG. 2. Left: Definition of the variables used in (1) to calculate the sticking probability $S(E, \xi)$ for an electron hitting a metallic solid with energy E and direction cosine $\xi = \cos \beta$. The probability for transmission through the surface potential is given by T while the probability for scattering inside the solid from a state (E, η) to a state (E', η') , where $\eta = \cos \theta$ and $\eta' = |\cos \theta'|$, is denoted by B . The metal is modelled by an exponential potential step characterized by a width parameter a and a depth $U_0 = E_F + \Phi$, where E_F is the Fermi energy and Φ is the work function. Also indicated is the electron energy distribution function $f_e(E)$ and the wall potential U_w an electron from the plasma has to overcome to reach the solid. Biasing the metal by $\pm V_{\text{bias}}$ would lead to $U_w \mp eV_{\text{bias}}$ while keeping E_F , Φ , and the origin of the energy axis fixed. Right: Electron emission yield $\text{EEY} = 1 - S(E, \xi)$ for $\xi = 1$ and a Ag surface characterized by $k_B T = 0.03$ eV, $E_F = 5.5$ eV, $\Phi = 4.4$ eV, $a = 0.26$ Å, and $n_{\text{imp}} = n/1000$, where n is the electron density corresponding to E_F . Electron-electron, electron-impurity, and electron-phonon scattering are taken into account. Using the electron-phonon coupling function $\lambda(E)$ as an energy dependent fit parameter, the experimental data [74] can be nicely reproduced. The dashed vertical line indicates the bulk plasmon energy, where nothing spectacular happens.

for the fact that the impacting electron cannot gain energy. The lower limits to the angle and energy integrals, $\eta_{\min}(E)$ and $E_{\min}(\eta')$, as well as the functions $\eta(\xi)$ and $\xi(\eta)$, which allow to switch between internal and external direction cosines, depend on the depth U_0 of the surface potential and the effective mass m_e^* of the electron in the conduction band of the metal. The functions arise from the conservation of lateral momentum and total energy.

In our previous work on dielectric surfaces [72, 73] the scattering cascades were driven by an optical phonon. Neglecting its dispersion, it was possible to approximately reduce the calculation of $B(E\eta|E'\eta')$ to the solution of an algebraic recursion relation. For metals, this is no longer possible because the finite density of electrons in the conduction band makes electron-electron collisions a main actor in the scattering cascades. The continuous energy losses which they give rise to cannot be treated algebraically. Since we found it necessary to also include electron-impurity and electron-phonon scattering, the theoretical treatment of metallic surface is quite involved. For the purpose of this perspective we describe the approach only as much as it is necessary to make our points. The technical details will be given elsewhere.

The function $B(E\eta|E'\eta')$ can be obtained from the invariant embedding principle for electron backscattering from surfaces [85–87] and a normalization procedure which takes into account that electron-electron scattering provides two possibilities for ending up in the final

state (E', η') , whereas for electron-impurity and electron-phonon scattering there is only one. The principle leads to an equation for the unnormalized backscattering probability $Q(E\eta|E'\eta')$. Forward and backward scattering events are encoded into different kernels, $K^+(E\eta|E'\eta')$ and $K^-(E\eta|E'\eta')$, respectively, which can be obtained from the golden rule scattering rates $W^+(E\eta|E'\eta')$ and $W^-(E\eta|E'\eta')$ and thus from the matrix elements for electron-electron, electron-impurity, and electron-phonon interaction.

To figure out which electronic states should be used in the matrix elements, a look at the universal curve for the mean free path of an electron inside a solid [88] is helpful. It suggests that an electron hitting a solid with energies below 100 eV, which is the range most important for plasma applications, penetrates rather deeply into the solid. The matrix elements, and also the transition rates, are thus the ones for bulk electronic states. Approximations which have been worked out for them can be also employed. In the high temperature limit, for instance, the rate for electron-phonon scattering reads in the quasi-elastic approximation [89],

$$W^\pm(E\eta|E'\eta') = \frac{\lambda(E)}{2} \frac{k_B T}{m_* k_F} \delta(E - E'), \quad (2)$$

where we used atomic units (measuring energy in Rydbergs, length in Bohr radii, and mass in electron masses) and introduced an energy dependent coupling function

$\lambda(E)$. In this approximation the rate does not depend on the direction cosines and the coupling function $\lambda(E)$ is all what remains from the electronic structure. The situation where an energy barrier prevents a primary electron with energy $E > 0$ from entering the solid, will be discussed in subsection III A. It occurs for surfaces with negative electron affinity.

The embedding approach separates forward and backward scattering. It is thus rather straightforward to take into account that forward scattering hardly changes the direction cosines. Assuming hence $K^+(E\eta|E'\eta')$ to be strongly peaked for $\eta = \eta'$, a saddle-point integration can be employed leading at the end to an integral equation for $Q(E\eta|E'\eta')$, where η and η' are only parameters. Suppressing them, the equation to be solved reads

$$\begin{aligned} Q(E|E') &= K^-(E|E') \\ &+ \int_{E'}^E dE'' K_1^+(E|E''; E') Q(E''|E') \\ &+ \int_{E'}^E dE'' Q(E|E'') K_2^+(E''|E'; E) \\ &+ \int_{E'}^E dE'' \int_{E'}^{E''} dE''' Q(E|E'') K^-(E''|E''') Q(E'''|E') . \end{aligned} \quad (3)$$

Two forward scattering kernels, K_1^+ and K_2^+ , appear because the saddle-point integrations leading to the second and the third term on the rhs were done with respect to different energy variables. Notice also, one of the three energy variables in K_1^+ and K_2^+ is always unaffected by the integrations.

To solve (3) numerically we expand $Q(E|E')$ in the number of backscattering events, that is, in powers of the kernel K^- . In each order, a linear Volterra-type integral equation has then to be solved. Empirically, we found for a silver surface convergence achieved at 17th order. Compared to dielectric surfaces, where we only had to solve an algebraic recursion relation, metallic surfaces are thus indeed computationally expensive. The details of the numerics do not matter at this point and will be described elsewhere. Important for the perspective is, the surface scattering problem is solved but its solution depends, via the kernels, on matrix elements entering the transition rates. The sticking coefficient depends in addition also on the surface potential, defining the quantum mechanical transition probability T . These are the quantities which have to be obtained either from first principle calculations or from surface diagnostics.

Let us now turn to results obtained for an electron hitting a silver surface with energies less than 20 eV, that is, with energies where the separation into true secondaries and backscattered electrons is no longer meaningful. Empirical formulae for the emission yield are thus not applicable. For the data shown, we statically screened the electron-electron and electron-impurity interaction. The coupling with phonons was considered in the quasi-elastic high-temperature approximation as discussed above. To

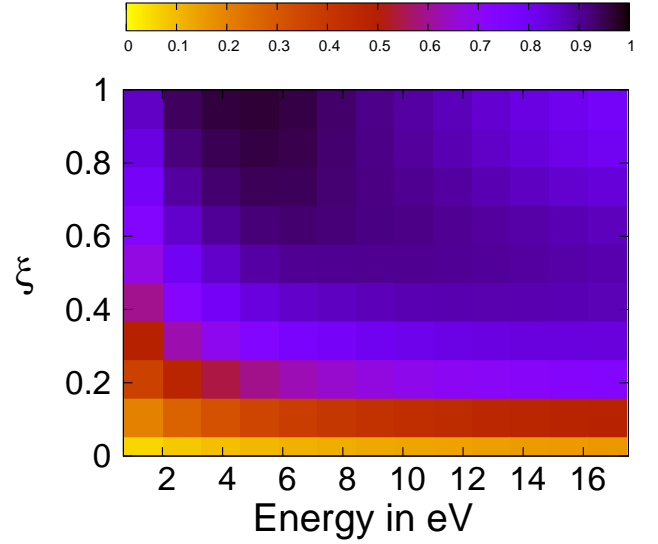


FIG. 3. Energy and angle dependence of the sticking probability $S(E, \xi)$ for the Ag surface specified in the caption of Fig. 2. In contrast to what one would expect, a metallic surface is not a perfect absorber for low energy electrons, that is, for electrons with energies below a few tens eV. Diffuse backscattering inside the metal makes the probability less than unity. It approaches unity only for $\xi = 1$ and $E \approx 5$ eV.

account for image charge effects, we used moreover an exponential surface barrier ($z < 0$, see Fig. 2),

$$V_s(z) = -\frac{U_0}{e^{-z/a} + 1} \quad (4)$$

with a width $a = 0.26 \text{ \AA}$ and a depth $U_0 = E_F + \Phi$, where $E_F = 5.5 \text{ eV}$ and $\Phi = 4.4 \text{ eV}$. The step potential also shown in Fig. 2 is recovered by setting $a = 0$. But it turned out not to be appropriate. Whereas E_F and Φ are at least known for free-standing Ag surfaces, the parameter a is essentially unknown. We use it therefore as a fit parameter. For $a = 0.26 \text{ \AA}$, we found best agreement with experimental data [74]. The model (4) could be avoided by knowing $V_s(z)$ either from first principle calculations or measurements. Since the plasma may chemically and structurally affect the surface, it may also modify $V_s(z)$. Calculations for $V_s(z)$ have thus to take the plasma into account and the experimental work concerning this quantity has to be done in-operando.

Figure 2 compares results for perpendicular incident with experimental data [74]. Since the data are for the electron emission yield, we plot $1 - S(E, \xi)$ instead of $S(E, \xi)$. The agreement with the data is rather good. To obtain it, we had to include electron-phonon scattering. Electron-electron scattering alone was not enough. The structure of (3) gives the reason. Being a Volterra-type integral equation, elastic backscattering, encoded into the diagonal $K^-(E|E)$, acts as a seed for the solution $Q(E|E')$ with $E \geq E'$. The elastic component of electron-electron scattering, however, is too weak. It is proportional to $k_B T / E_F$. To get the scattering cascade

running, other scattering processes are thus necessary. Electron-impurity scattering is also rather weak, at least for reasonable impurity concentrations. In the absence of Rutherford scattering on the nuclei (which may play a role), it is thus the interplay of electron-phonon and electron-electron interaction which affects most strongly the probability with which an electron scatters off a metal surface at low energies. We used the electron-phonon coupling function $\lambda(E)$ as an energy dependent fit parameter. For the results shown, $\lambda(E) = 0.1, 0.3$, and 0.5 for $0 < E < 5$ eV, $5 \leq E < 8$ eV, and $E \geq 8$ eV consistent with values expected from studies of electron heating in solids [90]. To avoid the empirical strategy, $\lambda(E)$ could be calculated from a model for electron-phonon interaction. Since the experimental data show no feature at the bulk plasmon energy, static screening of the Coulomb interaction seems to be in order. Although at room temperature electron-phonon dominates electron-impurity scattering, we kept the latter for completeness assuming an impurity concentration of $n_{\text{imp}} = n/1000$, where n is the electron density in the conduction band of Ag which can be obtained from E_F . But it actually has no effect on the results.

For the parameters reproducing the experimental data [74] we also calculated the angle dependence of $S(E, \xi)$ for the whole range $0 < \xi \leq 1$. It is shown in Fig. 3. The result is rather coarse grained but a finer grid would have increased the numerical costs dramatically. For almost all angles and energies $S(E, \xi)$ is less than unity. Only for $\xi = 1$ and $E \approx 5$ eV is S close to unity. Even a metallic Ag surface is thus no perfect absorber for electrons. In preliminary calculations we obtained similar good results for Cu and Au indicating that the semiempirical model captures the essential physics involved in the backscattering of low energy electrons from metallic surfaces. Combined with first-principle calculations or measurements of the surface potential $V_s(z)$ and the electron-phonon coupling function $\lambda(E)$ we expect the model to yield reliable electron sticking coefficients also for other metals. Since the original version of the model has already shown its usefulness for dielectrics [72, 73], the lack of experimental data for $S(E, \xi)$ could indeed be compensated by calculations of the type described in this subsection.

B. Kinetics of the electric double layer

From a plasma physics point of view, it is tempting to ignore the solid-state physics behind the surface parameters. For instance, the scattering cascades discussed in the previous subsection determining $S(E, \xi)$ are not part of traditional plasma modeling. The same holds for the microscopic processes determining secondary electron emission due to impacting heavy particles. In both cases, the physics is outsourced to specialists. The prospect, however, to calculate parameters which eventually are only buried in a plasma simulation, acquiring thereby a

merely supporting character, is not too motivating. More rewarding, and hence motivating, for condensed matter theorists is to overcome the parameters and to attempt a holistic modeling of the plasma-solid interface. It is then at least conceivable to discover so far overlooked scenarios arising from the interplay of processes taking place, respectively, in the solid and the plasma. Getting away from supporting-type calculations, we now consider the electronics inside plasma-facing solids as an integral part of the physical inquiry, to be studied at the same footing as the charge dynamics of the plasma it is bounding.

For this type of modeling electron sticking and secondary emission coefficients (due to electron impact) are obsolete. All what is needed is the quantum-mechanical probability T for an electron crossing the surface potential $V_s(z)$. We expect the holistic approach to be particularly rewarding for semiconductor-based miniaturized microdischarges [41] which are closest to the interest of solid-state physicists. In these systems transit times across the gas volume may be soon on the same order as the transport times inside the solid. Between two subsequent electron encounters the solid may thus stay in an excited state. Electron reflection and sticking should hence depend on this state.

In passing let us be a bit more basic by pointing out a fundamental difference between quantities characterizing collisions in the volume of the plasma (cross sections) and quantities describing collisions with the solid embracing the plasma (surface parameters). The former can always be calculated without considering the plasma environment. They are independent of it. Surface parameters, in contrast, may depend on it, because the plasma may in principle modify the surface chemically, structurally, and electrically. Rigorously speaking, the calculation of surface parameters has thus to take the plasma into account. The feedback of the plasma onto the surface parameters may be small in some instances. But from a fundamental point of view it is always there. For the calculation of the sticking coefficient, for instance, the modifications of the surface's electronic structure due to the plasma has to be considered. It is this modification which is the main theme of this perspective.

The set of equations for the holistic modeling of the charge dynamics on both sides of the plasma-solid interface consists of Boltzmann equations for the distribution functions of the involved charge carriers, the Poisson equation for the electric field, and matching conditions at the interface. For the dielectric plasma-solid interface shown in Fig. 4, the equations read (again in atomic units measuring energy in Rydbergs, length in Bohr radii, and mass in electron masses) [44, 48]

$$\left[\pm v_s(z, E, K) \frac{\partial}{\partial z} + \gamma_s(z, E, K) \right] F_s^{\pm}(z, E, K) = \Phi_s^{\pm}(z), \quad (5)$$

$$\frac{d}{dz} \varepsilon(z) \frac{d}{dz} U_c(z) = 8\pi n(z), \quad (6)$$

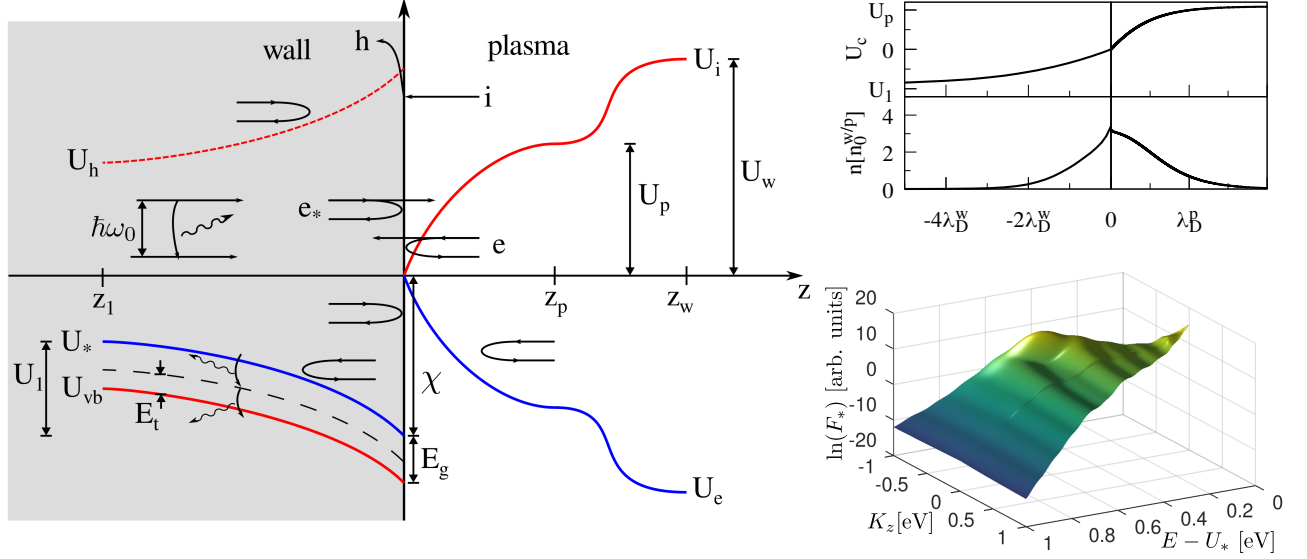


FIG. 4. Left: Interface model for an electric double layer with negative space charge inside the solid and positive charge in front of it. Shown are the edges of the conduction band (U_*) and valence band (U_{vb}), the edges for the motion of valence band holes (U_h), and the potential energies for electrons (U_e) and ions (U_i) on the plasma side. Hole injection due to the neutralization of ions, electron/hole-phonon scattering, and electron-hole recombination via traps in the energy gap are also illustrated together with reflection and transmission (where it applies) at the potential profile and the interface. The wall (sheath) potential on the plasma side is U_p while $U_w - U_p$ is the potential drop due to the plasma source at $z = z_w$. Right: Potential energy and net charge density profiles (upper panel) and distribution function for the surplus electrons inside the solid at $z = 0.13 \lambda_D^w$ (lower panel) as obtained from the numerical solution of (5) and (6) with the matching and boundary conditions specified in the text. On the solid (plasma) side, the potential is given in units of the band bending (sheath potential), $U_1 = -0.1$ eV and $U_p = 4.7$ eV, respectively, and the densities are given in units of $n_0^w = -10^{13} \text{ cm}^{-3}$ and $n_0^p = 5 \cdot 10^{13} \text{ cm}^{-3}$. Distances from the interface are measured in units of $\lambda_D^w = 0.29 \text{ } \mu\text{m}$ and $\lambda_D^p = 3.7 \text{ } \mu\text{m}$. The model parameters are given in Table I.

where we introduced distribution functions F_s^{\lessgtr} for left ($<$) and right ($>$) moving particles having, respectively, negative and positive velocity components in z -direction, and split the collision integral in an out-scattering and an in-scattering term, γ_s and Φ_s^{\lessgtr} , respectively. The index $s = *, h, e, i$, denotes, respectively, conduction band electrons, valence band holes, electrons, and ions. Independent variables are the spatial coordinate z perpendicular to the interface, the total energy E , and the kinetic energy K in the lateral dimensions. The function

$$v_s(z, E, K) = 2\sqrt{m_s^{-1}[E - U_s(z) - K]} \quad (7)$$

is the magnitude of the velocity perpendicular to the interface with $U_i = U_c$, $U_e = -U_c$, $U_* = -U_c - \chi$, and $U_h = U_c + E_g + \chi$ the potential energies for ions, electrons, conduction band electrons, and valence band holes. The source $n(z)$ of the Poisson equation is the charge distribution of the double layer consisting of a net negative (positive) charge inside the solid (plasma) to be selfconsistently obtained from the distribution functions.

To complete the set of equations we need conditions for matching the half-space solutions for the solid ($z < 0$) and the plasma ($z > 0$) at the interface ($z = 0$). For the electric potential energy U_c the standard continuity

conditions of electrostatics apply, while the distributions functions obey

$$F_{e,*}^{>,<}(0, E, K) = [1 - T(E, K)]F_{e,*}^{<,>}(0, E, K) + T(E, K)F_{*,e}^{>,<}(0, E, K), \quad (8)$$

$$F_h^{<}(0, E, K) = F_h^{>}(0, E, K) + S_h^{<}(E, K), \quad (9)$$

$$F_i^{>}(0, E, K) = 0, \quad (10)$$

where $T(E, K)$ is the quantum-mechanical electron transmission coefficient for the surface potential $V_s(z)$ and $S_h^{<}(E, K)$ is a function describing the injection of a valence band hole due to neutralization of an ion. For simplicity it is assumed that an ion hitting the surface is resonantly neutralized with unit probability but Auger neutralization could be also included. The source function $S_h^{<}(E, K)$ requires a model for hole injection and a normalization to ensure the equality of electron and ion fluxes at the interface, $j_e(0) = j_i(0)$, which has to be also satisfies. Augmented by boundary conditions, ensuring quasi-neutrality and the absence of electric fields in the bulk regions of the solid and the plasma, respectively, as well as plasma generation on the plasma side of the interface, the equations encode the chain of events shown in Fig. 1. Since the scattering inside the solid may bring electrons back to the interface, where they may be transmitted to the plasma, the electron emission yield and its

complement, the sticking coefficient, could be also obtained from the present scheme.

So far we considered a floating dielectric solid in contact with a plasma, keeping the model as simple as possible without affecting its main mechanisms. Details can be found in the literature [44]. For the purpose of this perspective it suffices to list its main features. The plasma is generated by a source selfconsistently attached deep inside the plasma by a standard construction [14]. The interface is perfectly absorbing from the plasma and impenetrable from the solid side. Due to numerical constraints, the energy domain is truncated, requiring to enclose electron and hole injection into effective (Gaussian) source functions, centered with a width Γ^{in} around $E - U_{*,h} = I_{*,h}^{\text{in}}$, below the actual injection points, which are too far above the band edges to be numerically accessible at the moment. The physics of the model is however unaffected by this construction. Collisions, finally, are only included on the solid side, where electrons and holes relax due to scattering on an optical phonon and recombine nonradiatively via traps in the energy gap of the dielectric. Again due to numerical constraints, at the moment we have to take an artificially high trap density. The plasma in front of the solid is collisionless. We also included a finite background doping by acceptors. Needless to say, the truncation of the energy domain as well as the high trap density can be avoided by investing into computing power.

Numerically the model can be solved by rewriting the kinetic equations (5) as integrals and applying an iterative approach initially developed for solid-solid interfaces [91–93]. Representative results are plotted on the rhs of Fig. 4 for the model parameters given in Table I. The absolute numbers, which depend on the truncations, are not of main concern at this point. More important is that a working scheme has been setup which extends the kinetic modeling into the solid. Let us first have a look at the potential and charge density profiles. Due to the difference in the Debye screening lengths, the charge neutrality of the double layer is not obvious from the plot but of course satisfied. The kink in the potential profile at $z = 0$ is due to the difference in the dielectric functions of the solid and the plasma, to be taken as $\varepsilon = 11.8$ and $\varepsilon = 1$, respectively. Also seen can be the band bending U_1 induced by the surplus electrons inside the plasma and the sheath potential U_p on the plasma side. The model determines both selfconsistently, together with the strength of the plasma source, which is also no more a free parameter but fixed by the scattering and recombination processes inside the solid [44].

The distribution function for the solid's surplus electrons originating from the plasma is plotted in the lower panel of the rhs of Fig. 4 for a spatial position immediately after the interface. Left- and right-moving distributions, $F_*^<$ and $F_*^>$, are distinguished by attaching an artificial sign to the variable $K_z = E - U_* - K$. Three features can be identified: (i) The peak at $E - U_* = 0.5$ eV due to electron injection, (ii) the replicas of this peak

TABLE I. Material parameters used to obtain the results shown on the rhs of Fig. 4. Conduction band electrons and valence band holes scatter on an optical phonon with energy $\hbar\omega_0$ and recombine nonradiatively via traps at energy E_t (measured with respect to the valence band edge), having a density N_t and a capture cross section σ_t . The dielectric has an energy gap E_g , an intrinsic density n_{int} , and is doped with an acceptor density n_A . As discussed in the text, we need source functions $S_{*,h}^<$ for injecting electrons and holes. They are defined in [44] and require the parameters Γ^{in} and $I_{*,h}^{\text{in}}$. The remaining parameters are the thermal energies and masses of the charge carriers.

$\hbar\omega_0$ [meV]	0.1
E_t [eV]	0.35
N_t [cm ⁻³]	10 ²⁰
σ_t [cm ²]	10 ⁻¹⁵
E_g [eV]	1
n_{int} [cm ⁻³]	5 · 10 ¹⁰
n_A [cm ⁻³]	10 ¹⁴
Γ^{in} [eV]	0.1
$I_{*,h}^{\text{in}}$ [eV]	0.5
$k_B T_{*,h,i}$ [eV]	0.025
$k_B T_e$ [eV]	2
$m_{*,h,e}$ [m_e]	1
m_i [m_e]	1836

due to electron-phonon scattering, and (iii) the step at $K_z = 0$, separating left- ($K_z < 0$) from right-moving ($K_z > 0$) electrons. Since the latter can only arise due to backscattering, which is less likely than forward scattering, the distribution function for right-moving electrons is suppressed compared to the distribution function for left-moving ones. Also seen is the overall decay of the distribution function in the variable $E - U_*$, signaling that the surplus electrons pile up at $E = U_*$, the bottom of the conduction band, and vanish high above it.

The overall picture encoded in Fig. 1 is thus nicely emerging from the kinetic theory spelled out in this section: Electron and ions created by a plasma source recombine inside the (dielectric) solid as conduction band electrons and valence band holes, after energy relaxation and transfer through the surface potential $V_s(z)$. The strength of the source is fixed by the electron microphysics inside the wall, which is thus of equal importance as the processes creating electrons and ions inside the plasma. Obviously, to set up this type of modeling, the electronic structure of the interface has to be known. It affects the electron transmission coefficient $T(E, K)$ as well as the scattering channels which have to be taken into account. For instance, in case surface states are present, surplus electrons may not only scatter into bulk states of the conduction band but also into surface states. Energy barriers, that is, the electron

affinity or the work function, are also affected by surface states because they are usually charged giving rise to band bendings and surface dipoles. Hence, a quantitative description of the double layer at a plasma-solid interface, in particular, of its solid-based part, requires input data which can be only obtained by making the electronic structure of plasma-facing solids the object of experimental and theoretical inquiry.

C. Infrared diagnostics for the wall charge

Based on assumptions about the electronic structure of a dielectric plasma-solid interface we presented in the previous section a kinetic theory which determines the distribution functions and the depth profiles of surplus electrons and holes making up the wall charge. To test and guide theoretical approaches of this kind, it is also necessary to access the wall charge by experimental techniques. So far, methods exist for measuring the accumulated charge per unit area by electric probes [23], optomechanical sensors [24], and the optoelectric Pockels effect [25]. The latter allows also to extract the lateral charge distribution [26, 27]. No attempts have been made, however, to measure charge profiles perpendicular to the interface or to determine the electronic states hosting the charge. Thermostimulated current [94] and luminescence [95, 96] techniques have been used to estimate the binding energy of an electron trapped in or onto a plasma-facing dielectric, but the electronic states involved could not be determined by them. Hence, there is a need to improve the charge diagnostics. In particular, it is necessary to make it microscopic enough to explore charge distributions inside the solid. Combined with theoretical modeling, the character of the electron states the wall charge is bound to (bulk vs. surface states) could then be also uncovered.

In this subsection we discuss the possibility of using infrared reflection spectroscopy as a diagnostics for the charge inside a plasma-facing dielectric material. In contrast to our previous proposals for using optical [97] or electron [98] spectroscopy to determine the charge of a planar plasma-facing solid, the new proposal does not rely on a from-the-back geometry and does also not require a layered structure. Instead, we now suggest to use the dielectric wall as an internal reflection element. The charge is thus determined by passing p-polarized infrared light directly through the wall. Since we base our analysis in addition also on surface response functions [99] we are now able to treat inhomogeneous charge distributions. The homogeneous Drude model we used previously for the charge residing in the wall can thus be avoided and with it the artificial confinement of the charge by layering the solid structure in contact with the plasma.

The idea of the proposal is shown on the lhs of Fig. 5. Infrared light passes through a dielectric parallelepiped which serves at the same time as the wall of the plasma. Provided the optical loss inside the dielectric is small, the

wall can be macroscopically thick and hence mechanically stable. The angle of the entrance surface is large enough to ensure total reflection at the plasma-solid interface. On the opposite interface the parallelepiped should be polished to ensure perfect reflectivity. Since total reflection at the plasma-solid interface depends on the dielectric function in the vicinity of the interface, and hence on the charge distribution around it, the intensity of the transmitted light should be sensitive to the wall charge. Indeed, exploratory calculations show the feasibility of the scheme. We will now present it in some detail hoping to motivate experimentalists to implement the approach.

In the incoherent limit, where the thickness of the optical element is much larger than the wavelength of the light, the transmissivity T of the element, that is, the ratio of the transmitted (I_T) to the incoming (I_0) light intensity is given by [100]

$$T = \frac{I_T}{I_0} = \frac{R_s^N (1 - R_0)^2}{1 - R_s^{2N} R_0^2} \quad (11)$$

with R_0 the reflectivity at the entrance and exit interface and R_s the reflectivity at the plasma-solid interface. Whereas R_0 is simply given by the Fresnel formula for perpendicular incident at a dielectric-vacuum interface, R_s is a non-Fresnel reflectivity for angle of incident θ . It takes the charge inhomogeneities at the dielectric-plasma interface into account. Compositional or structural inhomogeneities could be also included. But we focus in this subsection only on the charge.

In order to calculate R_s we employ an approach based on surface response functions [99]. Indexing the materials as shown in Fig. 5 and denoting Fresnel reflection coefficients between media i and j by \bar{r}_{ij} , the reflectivity at the entrance and exit interfaces reads $R_0 = |\bar{r}_{12}|^2$, while $R_s = |r_{23}|^2$ with (suppressing the $\omega = 2\pi c/\lambda$ dependence where it applies) [99]

$$r_{23} = \bar{r}_{23}(1 + C_{23}) \quad (12)$$

and

$$C_{23} = 2ip_2 \frac{p_3^2 \bar{\varepsilon}_2 d_{\parallel} - k^2 \bar{\varepsilon}_3 d_{\perp}}{\bar{\varepsilon}_2 p_3^2 - \bar{\varepsilon}_3 k^2}, \quad (13)$$

where $\bar{\varepsilon}_i$ and p_i denote the (homogeneous) bulk dielectric function and the perpendicular component of the wavevector of the light in medium i , k is the conserved parallel component of the wavevector, and

$$d_{\perp} = \frac{\int dz \{ \varepsilon_{zz}^{-1}(z) - [\bar{\varepsilon}_2^{-1} \theta(-z) + \bar{\varepsilon}_3^{-1} \theta(z)] \}}{\bar{\varepsilon}_2^{-1} - \bar{\varepsilon}_3^{-1}} \quad (14)$$

$$d_{\parallel} = \frac{\int dz \{ \varepsilon_{xx}(z) - [\bar{\varepsilon}_2 \theta(-z) + \bar{\varepsilon}_3 \theta(z)] \}}{\bar{\varepsilon}_2 - \bar{\varepsilon}_3} \quad (15)$$

are the surface response functions. They depend on integrals,

$$\varepsilon_{xx}(z) = \int dz' \varepsilon_{xx}(z, z'), \quad (16)$$

$$\varepsilon_{zz}^{-1}(z) = \int dz' \varepsilon_{zz}^{-1}(z, z'), \quad (17)$$

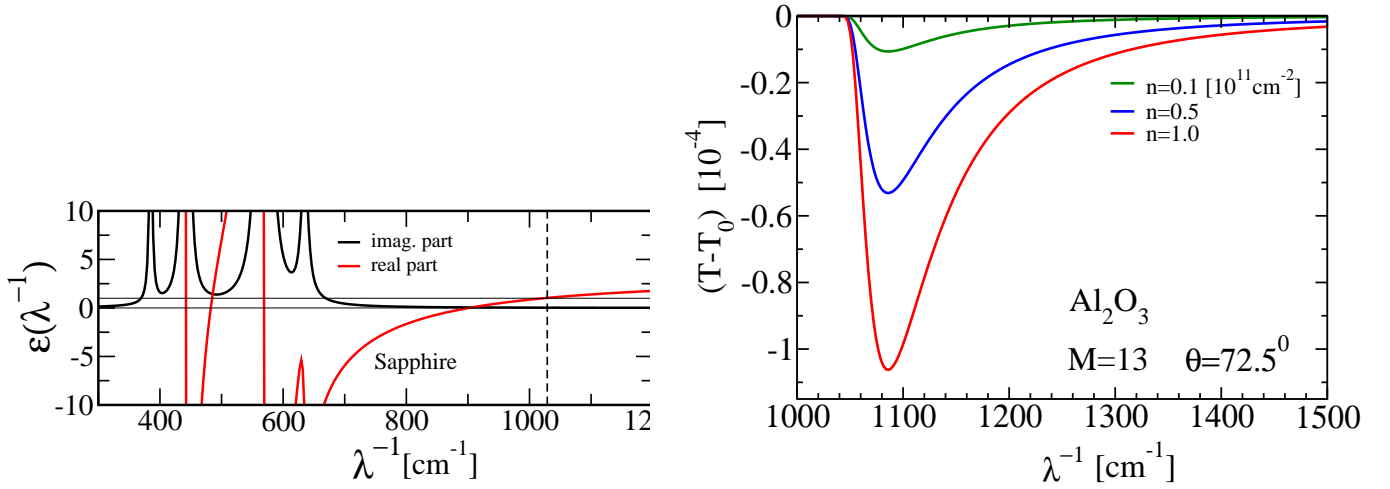


FIG. 5. Left: Principle of the experimental setup for measuring the charge accumulated inside a plasma-facing dielectric by infrared spectroscopy. The transmitted light through the dielectric serving as an internal reflection element is detected in the vicinity of the wave number where internal reflection sets in, that is, where the real part of the dielectric function becomes larger than unity. For sapphire $\lambda^{-1} \approx 1040 \text{ cm}^{-1}$ (see dashed line in the plot for $\epsilon(\lambda^{-1})$). Right: Theoretically predicted change of transmissivity $\Delta T = T - T_0$, where T and T_0 are, respectively, the transmissivities for plasma-on and plasma-off, as a function of n_s for a reflection element made out of sapphire. Fitting experimental data for ΔT to theoretical curves, arising as discussed in the main text from models for the space charge layer inside the solid, will enable one to determine $n_s = \int dz n(z)$ and maybe even the charge density profile $n(z)$ itself.

over the nonlocal dielectric function (and its inverse) containing the charge inhomogeneity via a Drude term. The z -integrals run over the dielectric ($z < 0$) as well as the plasma halfspace ($z > 0$).

The central object is the dielectric function. In tensor notation with respect to the spatial coordinates,

$$\underline{\epsilon}(z, z') = \underline{1}\delta(z - z') [\bar{\epsilon}_2 \theta(-z) + \bar{\epsilon}_3 \theta(z)] + \frac{4\pi i}{\omega} \underline{\sigma}(z, z'), \quad (18)$$

where $\underline{\sigma}(z, z')$ is the conductivity tensor. It can be obtained from the kinetic theory described in the previous subsection by including an additional force term due to the electric field of the infrared light send through the wall and linearizing the new set of Boltzmann equations around the solution of the electric double layer. From the electric current produced by this procedure $\underline{\sigma}(z, z')$ can be identified. The dielectric function follows straight and its inverse can be obtained numerically.

We did not yet implement the full scheme. To obtain first results we adopted a local approximation. Under the assumption that the charge inhomogeneities are due entirely to conduction band electrons and ions on the solid and plasma side of the interface, respectively, we write

$$\underline{\epsilon}(z, z') = \underline{1}\delta(z - z') [\epsilon_2 \theta(-z) + \epsilon_3 \theta(z)] \quad (19)$$

with

$$\epsilon_i = \bar{\epsilon}_i - \frac{4\pi e^2}{m_i} n_i(z), \quad (20)$$

where $m_2 = m_*$, $m_3 = m_+$, $n_2(z) = n_*(z)$, and $n_3(z) = n_+(z)$. Going through the formulae for the surface response functions (14) and (15), one realizes that for $m_+ \gg m_*$ the integrals over the plasma side of the interface can be neglected in leading order. The functions depend then only on $n_*(z)$. Using, for purpose of demonstration, a rough model $n_*(z) \sim e^{z/a}$, the integrals can be work out easily. Normalizing finally $n_*(z)$ over the width of the reflection element to a total surface density n_s , we get at the end the transmissivity (11) as a function of n_s .

Results obtained for this simple model are shown on the rhs of Fig. 5. The wavenumbers of interest are the ones around the threshold for total reflection at the plasma-solid interface, defined by $\bar{\epsilon}(\lambda^{-1}) = 1$. Taking sapphire as an example, $\lambda^{-1} \approx 1040 \text{ cm}^{-1}$, as can be seen from the dielectric function on the left. To determine n_s experimentally, it is best to focus on the change of transmissivity when the plasma is turned on. For plasma off, $n_s = 0$ and—since we neglect other possibilities of inhomogeneities— $R_s = \bar{R}_s = |\bar{r}_{23}|^2$, while for plasma on $R_s = \bar{R}_s |1 + C_{23}|^2$. Inserted into (11) two transmissivities, T and T_0 , result whose difference $\Delta T = T - T_0$ is shown on the right. A clear signature can be observed for values of n_s typical for dielectric barrier discharges. The magnitude of ΔT is in this example rather small, but a photodetector with a high enough sensitivity should be able to measure it. In other applications of reflection spectroscopy, sensitivities up to 10^{-3} have been achieved decades ago [67, 101]. We expect modern instrumentation to be actually better and are thus convinced that the proposed method can be realized. It is also conceivable

to place the optical element between two highly reflecting mirrors and to measure the absorbance $A = -\log T$ of the element by cavity ring down spectroscopy [102] which is known to be an extremely sensitive technique. The mirrors can be also integrated into the optical element itself [57, 61, 62] by coating the entrance and exit interfaces appropriately. In the next section we will say more about this particular technique because it can be perhaps also applied to investigate in-operando the infrared active parts of the electronics of plasma-facing solids.

The advantage of the charge diagnostics described in this subsection is that it requires only the material to be transparent for infrared light. Many dielectrics of interest for plasma applications obey this criterion. With this type of spectroscopy, it is also possible to monitor in-operando chemical and structural modifications of the plasma-solid interface, which in general lead also to changes in the dielectric function around the interface and hence to non-Fresnel reflectivities from which information about the modifications is gained. For that purpose the standard modus of operating reflection spectroscopy is employed: looking for changes in transmissivity above the threshold for total reflection at the plasma-solid interface. The charge diagnostics, on the other hand, focuses on changes close to the threshold.

III. WORK WE HOPE TO INITIATE

In the previous section we continued our ongoing research program on electron kinetics at plasma-solid interfaces, comprising the calculation of surface parameters, the modeling of the electric double layer, and a proposal to measure the solid-bound part of the double layer by infrared reflectivity. The models on which our work is based employ parameters and functions associated with the electronic structure of the plasma-facing solid. Particularly important are energy barriers, that is, for metals the work function and for dielectrics the electron affinity. For the calculation of the electron sticking coefficient, the shape of the surface potential and the electron-phonon coupling function turned out to be also essential, while the modeling of the electric double layer required, among others, information about recombination cross sections and trap densities. All these quantities are related to the electronic structure of the plasma-facing solid. To make the models predictive, it is thus necessary to know as much as possible about it, either from experiment or ab-initio theory.

First-principle calculations of the electronic structure are only practical for properties which are not affected by the presence of the plasma. The electron-phonon coupling function used in the calculation of the electron sticking coefficient, for instance, is such a quantity. It depends only on the bulk electronic structure which is shielded from the influence of the plasma. Energy barriers, in contrast, are not. They depend on what the plasma initiates chemically and structurally on the sur-

face. A calculation of the barriers requires therefore to treat the interaction between a plasma and a solid in all its electrical, structural, and chemical manifestations. A hopeless endeavor—at least if it is unguided by experimental investigations of the electronics, structure, and chemistry of the interfaces.

More promising is to determine the information about the electronic structure of the plasma-solid interface experimentally by photon and electron spectroscopy [49]. Energy barriers, the energetic position of surface states, and the surface potential, to name only the most important electronic interface parameters, can be for instance measured by photoemission spectroscopy. Up to now, this type of spectroscopy has neither been performed ex-sito (plasma off) nor in-operando (plasma on) on a plasma-facing solid. Both modii are challenging because the sample to be investigated is outside the vacuum equipment required for the electron beams part of the interface diagnostics. Primarily because in-operando techniques can also provide information about the depth profile of the wall charge, we argue in this subsection for setting up in-operando experiments. Although more complicated than ex-sito experiments, they would yield insights about the electronics of the plasma-solid interface which we never had before.

A. Motivation for in-operando diagnostics

Besides being able to explore the profile of the wall charge there is also a fundamental reason favoring in-operando over ex-sito characterizations of the plasma-solid interface.

The electronic structure of a surface is a thermodynamic property, arising from the minimization of its free energy [103]. As a result, the positions and bondings of the atoms in the first few crystallographic planes of the surface usually differ from the ones appearing in the simply truncated corresponding solid. It is this reconstruction of the surface which determines the electronic structure and hence also the energy barriers electrons have to overcome if they want to enter or leave the solid. The plasma exposure affects of course the positions of the atoms on the surface, due to particle and energy influx. The minimization of the free energy the surface has to perform is thus constrained by the plasma. It could thus well be that the in-operando electronic structure of a plasma-facing solid strongly deviates from its ex-sito counterpart. Characterizing it ex-sito may thus not be sufficient.

To motivate in-operando experiments further let us have a look at the electronics which may take place at plasma-facing dielectrics. Due to their relevance for solid-bound microdischarges [40–43] we focus on this class of materials.

The electronic structure of a dielectric surface is strongly affected by its termination. Particularly the presence of surface states depends on it, which in turn

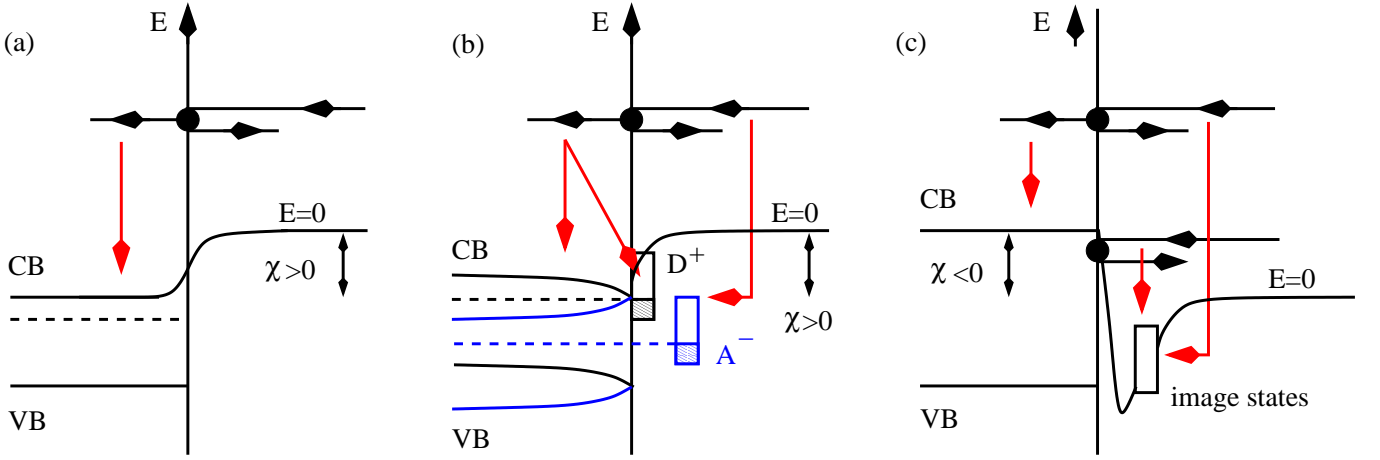


FIG. 6. Illustration of three possibilities for the band structure of a dielectric surface. Which one may be realized depends on the plasma exposure. (a) Positive electron affinity without surface states. The model we currently employ. (b) Positive electron affinity with surface donors (D^+) or acceptors (A^-) leading to band bending. (c) Negative electron affinity leading to image states in front of the surface. In situations (b) and (c), the impinging electron may also scatter into the respective surface states. As in Fig. 2, the origin of the energy axis coincides with the potential just out-side the surface.

affects the distribution of intrinsic and extrinsic charges across the surface. The former may lead to a surface dipole, and hence to a modification of the energy barrier an electron has to overcome by leaving or entering the solid, while the latter concerns the solid-bound part of the double layer. Surface states may also open up additional channels for electron capture from the plasma. As shown in Fig. 6, an electron impinging on an interface with surface states may not only scatter into bulk states (as assumed in subsection II A) but also into acceptor-like (A^-) or donor-like (D^+) states at the interface. Besides a wide space charge layer, the negative leg of the double layer may thus also consist of a strongly localized part. A particularly interesting situation arises for dielectrics with negative electron affinity, where electrons may be trapped in front of the surface by polarization-induced image states [104, 105], not unlike to what happens to electrons on top of a liquid helium film [106]. Materials with this property are diamond [107–109], boron nitride [110], and MgO [111, 112]. Since the plasma affects the termination of a plasma-facing dielectric chemically as well as structurally, its electronic structure, especially the important class of surface states, will depend on the plasma. It thus has to be studied in-operando.

To make this point more explicit let us discuss ZnO as an example [113, 114]. From band structure calculations it is known that the electronic structures of reconstructed and non-reconstructed ZnO surfaces are different [113]. In particular, the energetic position of the surface states depends on the organization of the atoms in the first few atomic layers. For the $(10\bar{1}0)$ surface this can be seen in Fig. 7. Since the energy and particle flux from the plasma disturbs the atoms in the top layers, the position of the surface state S_1 may change in the course of plasma exposure. The state may be even absent and the in-operando electronic structure completely different from

the one of the free-standing reconstructed $(10\bar{1}0)$ ZnO surface. Only in-operando diagnostics could tell if this is indeed the case. Chemical modifications of the electronic structure of a plasma-facing ZnO surface are also conceivable. Adlayers of H-atoms and OH-groups, for instance, affect the band bending at a ZnO surface [114]. Traces of these substances inside the plasma will thus most probably influence the electron kinetics across a plasma-ZnO interface –via the surface states the band bending must be associated with, which in turn also affect energy barriers and capture cross sections. In-operando techniques could provide information about the chemically modified electron kinetics at the plasma-ZnO interface even if the adlayers are only present while the plasma is on.

Having argued up to this point that the modeling of the electron microphysics at the plasma-solid interface depends on the in-operando electronic structure of the plasma-facing solid, and hence it should be investigated experimentally, the question remains, are the experiments good for anything more than only providing input parameter for the modeling. In our view, they are because they may help to establish a new research arena at the intersection of plasma and surface physics.

In this arena it would be possible, for instance, to work towards designing the electric properties of plasma-solid interfaces by a judicious choice of the solid and the feed-stock gas. The interface resistance could perhaps be engineered as well as the shape of the double layer. Material science provides an almost inexhaustible reservoir of materials with surfaces having rather sensitive electronic structures. Subjecting them to various low-temperature plasmas could be part of a systematic search for discharges with new operation modii or functionalities.

We already listed materials with negative electron affinity. Especially diamond, whose electron affinity can be tuned chemically from positive to negative [115–117],

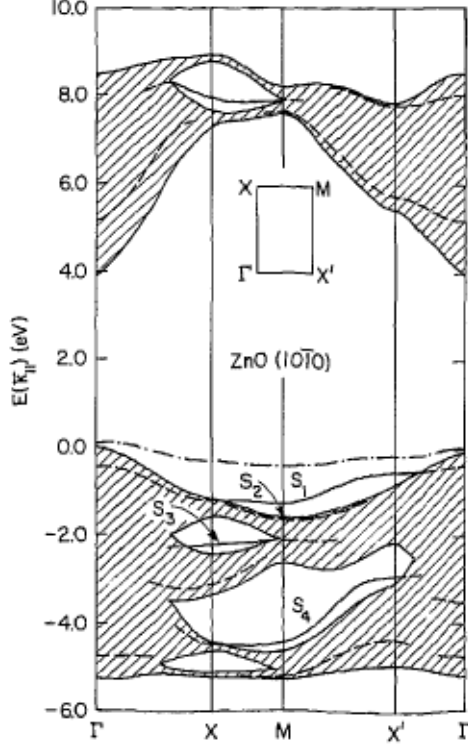


FIG. 7. Example for the dependence of the energetic position of a surface state on the arrangement of the atoms in the first few atomic layers, that is, on the reconstruction of the surface. Shown is the band structure for the $(10\bar{1}0)$ surface of ZnO together with its Brillouin zone. The position of the surface state S_1 near the top of the valence band before (after) reconstruction is indicated by the dot-dashed (solid) line. The reconstructed surface has further surface states S_i (solid lines) as well as surface resonances (dashed lines). Anticipating now the $(10\bar{1}0)$ ZnO surface is exposed to a plasma. Due to the permanent influx of energy and particles, the geometric ordering of the surface atoms is not clear. Hence, it is uncertain where, if present at all, in the in-operando band structure the surface state S_1 will be sitting. Adapted with permission from Wang and Duke, *Surf. Sci.* **192**, 309 (1987) [113].

is an interesting candidate for establishing new types of low-temperature gas discharges. The tuning of the electron affinity can very well be performed by the plasma itself. It is thus conceivable to come up with a plasma-diamond interface with tailor-made electron affinity and hence electron microphysics. Using diamond layers in a dielectric barrier discharge and tuning the electron affinity from positive to negative by changing the chemical composition of the feedstock gas, while simultaneously measuring the electron affinity and some key plasma parameters, could be a research project in this new arena.

Another project could involve the photocatalyst TiO_2 . The electronic structure of its surface can be controlled by oxygen and UV light [118, 119]. Using TiO_2 in a

barrier discharge, whose feedstock gas contains traces of oxygen, and monitoring its electronic structure together with the plasma may thus be also an interesting study. Many more projects are conceivable and could be performed once the tools of in-operando interface diagnostics are in place.

B. Implementation of in-operando diagnostics

Experimental probes most suited for investigating the geometry, chemical composition, and electronic structure of free-standing surfaces are electron and photon spectroscopy [49]. Applying them in-operando also to plasma-facing solids would yield a host of data we so far have no access to. Unfortunately, the presence of the plasma prevents the techniques to be applied directly to the interface of interest. The electric field in the sheath disturbs incoming and outgoing electron beams making electron and photoemission spectroscopy (which involves an outgoing electron) from the front impossible. The standard setups do not work. Thus, one has to come up with alternatives. Two are shown in Fig. 8: The spinning wall [66] and the from-the-back geometry.

Let us first discuss the spinning wall technique. It is shown on the lhs of Fig. 8 and has proven its feasibility for in-operando Auger electron spectroscopy [66]. We expect it therefore to be also suitable for other types of electron and photon spectroscopy. In particular, photoemission spectroscopy [49] for chemical, structural, and electronic analysis could be performed in such a setup. The trick of the wall is to alternately expose the surface to the plasma environment and the vacuum necessary for its diagnostics. The simplest way to do this is to use a cylinder made out of (or covered with) the material to be studied, place it properly sealed inside the wall of the discharge vessel, and rotate it with a constant velocity. Since the diameter of the cylinder is a few cm, on the atomic scale the surface remains flat. The photon beam hitting in a photoemission study the circumference of the cylinder on the vacuum side of the device, and hence in the standard manner, probes thus an atomically flat surface. It may thus even be possible to investigate it by photoemission electron microscopy [120].

A drawback of the spinning wall is that it is only in-operando for plasma-induced processes persisting at least for the time a full rotation takes. The modification of the surface due to the plasma, be it chemical, structural or electrical, should also not be undone by passing through the seals. For the rotation velocity used in the Auger electron diagnostics of the plasma wall [66], processes decaying slower than a few milliseconds could de-facto be observed in-operando. Chemical desorption takes place on a much longer time scale. Hence, chemical modifications due to adlayers and the changes in the electronic structure they give rise to (energy barriers, band bending etc.) stay intact during the rotation and should thus be observable by this technique. Provided surplus elec-

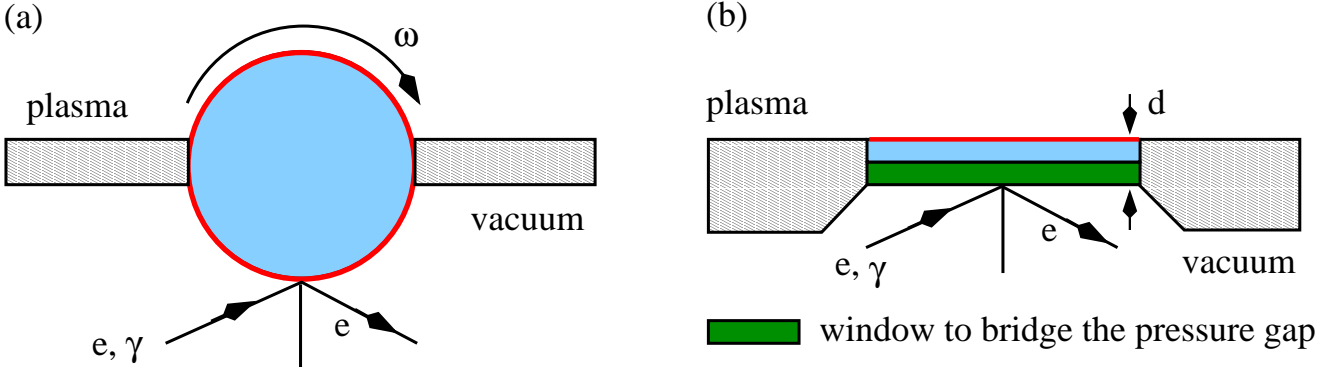


FIG. 8. Two possibilities for performing in-operando photoemission and electron energy loss spectroscopy of a plasma-facing solid. (a) Spinning wall setup [66] and (b) from-the-back geometry. In photoemission spectroscopy a photon (γ) of fixed energy excites the electronic system of the target. The information about its electronic structure is then encoded into photoelectrons as well as secondary electrons. Electron energy loss spectroscopy, on the other hand, is an electron reflection technique. It utilizes the coupling of the incoming electron (e) to the dipole fields of the charge fluctuations inside the target. Detecting the nearly specularly reflected electron beam enables then to read out information about the charge distributions. The thick red line indicates the interface of interest.

trons making up the wall charge stay long enough on the surface, the spinning wall can be also used to measure their total amount per unit area by electron energy loss spectroscopy to be discussed at the end of this section. Indeed, electron residence times on dielectric surfaces can be very long. On a bismuth silicon oxide (BSO) [27] or a sapphire [95, 96] surface, for instance, some electrons appear to be trapped for at least minutes, long enough to be even measurable by ex-situ setups, that is, when the plasma is off. The depth profile of the wall charge, however, a quantity we are particularly interested in, cannot be determined by a spinning wall setup since the restoring force of the sheath, which affects the profile, is absent when the surface is on the vacuum side for diagnostics. It may be however explored in a from-the-back geometry to which we now turn.

Such a setup is shown on the rhs of Fig. 8. It is based on a layered structure, which is thin enough to allow information about the plasma-solid interface to be read out from the interface opposite to it and at the same time thick enough to guarantee mechanical stability. Experimentally, one now faces the problem of investigating a buried interface. The progress made in this field, especially with respect to buried liquid-solid [50, 51, 53, 54] and solid-solid [55, 56, 58–60] interfaces, where information depths up to 70 nm have been realized [56], makes us rather optimistic that the from-the-back setup may actually work for the plasma-solid interface.

The challenge is to have an information depth large enough to allow structures to be build which are also mechanically stable. Since in photoemission spectroscopy the information is carried by electrons, the thickness of the stack cannot exceed the inelastic mean free path for an electron. From the universal curve [88] it then follows that, if at all, the method may work for electrons with rather low or rather high energy. For them the mean free paths are longest, on the order of 10 – 100 monolayers. In

practice, the method is thus limited to sub-100 nm thick structures and electron energies of a few eV or a few keV. The mechanical stability of sub-100 nm thick structures is obviously a critical issue. Fortunately, there are materials such as SiO_2 , Al_2O_3 , and Si_3N_4 which are hard and robust enough to make such a setup conceivable. In particular, Si_3N_4 has proven its usefulness as a sub-100 nm window in from-the-back microscopy at vacuum-liquid [58] as well as vacuum-plasma interfaces [63, 65]. It could thus be coated with the material of interest and inserted into the wall as shown on the rhs of Fig. 8.

A number of technical details beyond mechanical stability have to be of course also clarified before experiments of this sort can be put into place. Not only the vacuum side of the setup, where the diagnostics takes place, has to be designed carefully. The plasma chamber with its recess for the measuring window needs also attention. In case the setup is utilized to study a floating plasma-solid interface, the recess has to be electrically isolated from the rest of the wall. The measuring window in turn has to be optimized by model calculations for different stacks of materials having various thicknesses. Ideally, the plasma-facing layer is thick enough for the wall charge to develop its full depth profile. Initially, however, the required thickness is unknown. It depends on the electronic structure of the plasma-facing solid the experiment is supposed to reveal. Based on assumptions about the electronic structure, model calculations can however estimate the depth. In an iterative process, involving calculations and measurements, the optimal configuration can hence be found.

With an optimized configuration for the measuring window the plasma-solid interface could be analyzed in-operando in the same manner as free-standing surfaces in the from-the-top geometry [49]. For instance, using hard X-rays in the keV energy range, the chemical composition could be analyzed. Depth-profiling of selected lines could

provide information about the band bending and hence about the surface potential and energy barriers. The filling of the electronic states at the interface could be studied by direct and inverse photoemission spectroscopy in the eV energy range, using ultraviolet light. It would thus be possible to determine for the first time the states hosting the wall charge.

Since we recently proposed from-the-back electron energy loss spectroscopy as a diagnostics for the wall charge [98], we also say a few words about this work. The setup is identical to the one shown on the rhs of Fig. 8. Instead of a photon the inquiring particle is an electron which however does not enter the solid structure. The electron mean free path is hence not the critical length scale for reading out information about the plasma-solid interface on the opposite side. Instead it is the range of the dipole fields of the charge fluctuations inside the solid which has to be comparable to the thickness of the stack for the from-the-back geometry to work. To avoid surface response functions, we assumed the wall charge to be homogeneously confined within the plasma-facing film by an electronegative substrate layer. The strength of the signal we found for a stack which we considered to be still mechanically stable, was however rather weak. Only by pre-doping the plasma-facing film with electrons the signal passed a plausible detection limit.

Whereas from-the-back electron energy loss spectroscopy does not look too promising, it may be feasible to do it with a spinning wall. There, while on the vacuum side, the interface is subjected to the electron beam directly. From-the-front, however, space charge layers have been successfully investigated by electron energy loss spectroscopy [121–123]. We expect therefore the spinning wall to enable electron energy loss spectroscopy of the wall charge. To determine the total magnitude of the wall charge per unit area, and possibly also the depth profile of the wall charge, a theoretical analysis of the measured signal is however necessary. Unlike to what we did in our exploratory work [98], the theoretical analysis has to take the charge inhomogeneity perpendicular to the interface into account. For that purpose, it is necessary to generalize the calculation of the cross section for electron energy loss [124] to non-Fresnel interfaces by combining it with surface response functions [99].

The in-operando diagnostics we focused on so far are of the type photon in and electron out (photon spectroscopy) or of the type electron in and electron out (electron energy loss spectroscopy). A technique employing only photons is infrared spectroscopy. In subsection II C we proposed to use it as a diagnostics for the wall charge. Especially in combination with the cavity ring down methodology [57, 61, 62, 102], we expect it to be rather sensitive. The ring down approach may be however also useful for studying in-operando the infrared active parts of the electronics of plasma-facing dielectrics. The setup for this purpose is identical to the one used for the in-growth investigation of dangling bonds in a hydrogenated amorphous silicon (a-Si:H) film [57, 61]. It is

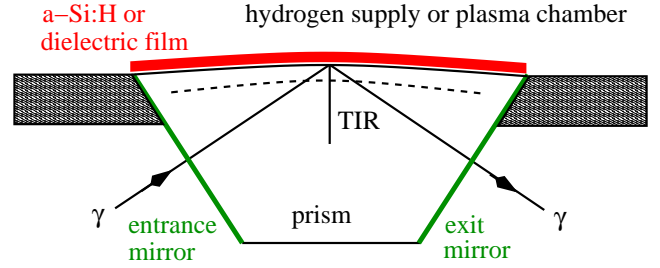


FIG. 9. Illustration of the setup used for studying dangling bonds in a-Si:H films during growth [57, 61]. The prism acts as a total internal reflection (TIR) element and as an optical cavity which is fed by an infrared pulse. Due to the evanescent field leaking from the cavity into the film additional optical losses occur. From the change of the pulse's ring down time information about the dangling bonds can be obtained. With a similar setup the infrared active parts of the electronics of a plasma-facing dielectric can be perhaps also investigated. The dielectric could be deposited as a film on top of the TIR side of the prism or used as the material from which the prism itself is made from. In the latter case, it is the absorbance of the propagating wave inside the prism which carries information about the in-operando modifications of its electronics. The dashed line indicates the region of the wall charge which we expect to be also measurable by such a setup.

schematically shown in Fig. 9, together with the labeling for the application we have in mind. The a-Si:H film is deposited on the total internal reflection (TIR) side of a prism which acts also as an optical cavity because of highly reflective coated entrance and exit interfaces. Due to the coupling of the dangling bonds to the evanescent electric field leaking from the prism into the film, light intensity is lost from the cavity. Exciting the prism by an optical pulse and tracking in time the optical losses of the prism provides thus information about the density [61] and kinetics [57] of the bonds while the film keeps growing.

As suggested by the labeling in Fig. 9 a similar setup can be perhaps used to investigate the infrared active parts of the electronics of a dielectric in contact with a plasma. Two operation modii are conceivable. Either one deposits the dielectric on top of the TIR side of the prism and utilizes the evanescent component of the electric field leaking out of the cavity, as it is done in the investigation of the a-Si:H film. This would be the canonical way to study a dielectric plasma-solid interface by evanescent wave cavity ring down spectroscopy [52, 62]. It has however the drawback to be limited to thin films. An alternative would be to use the dielectric of interest itself as a prism material. Since most dielectrics are transparent in the infrared this should be possible. It would then be the plasma-induced change of the absorbance of the propagating wave inside the prism, caused, for instance, by surplus carriers in the space charge layer (wall charge) or by modifications of the subgap defect or surface states, which affects the ring down time of the cavity. Using—by construction—the plasma-facing dielectric as an

optical element in the infrared should thus provide access to the infrared active parts of its electronics. The measurements can be done while the plasma is on, an in-operando investigation should hence be possible.

Again, numerous technical details have to be clarified before experiments of this sort can start. For instance, the spectral range of the light which can be coupled into the cavity depends on its eigenmodes and thus on the geometry of the prism which hence has to be constructed carefully. The light pulses have to be moreover short enough to enable a detection of the ring down time. In addition, the relative weight of the absorbance in the bulk and the interface regions of the prism has to be quantified. Only the latter provides information about the electronic structure of the plasma-solid interface. To what extend this can be done within the framework of generalized reflectivities introduced in subsection II C is an open issue and should be part of theoretical studies guiding the planning of the experiments.

IV. SYNOPSIS

Traditionally, in plasma physics, the electron microphysics at plasma-solid interfaces is associated with probabilities for electron deposition and extraction. The in-operando electronic structure of the interface, which also includes its charging due to the plasma, has so far not been the subject of systematic investigations. Yet, it is intrinsically coupled to the plasma due to particle and energy influx. Knowing the interface's in-operando electronic structure—in contrast to the electronic structure of the solid without plasma exposure—seems to us essential for taping the full technological potential of bounded low-temperature gas discharges. Particularly the electric properties of miniaturized solid-based dielectric barrier discharges call for an in-operando investigation, since the solid becomes an integral part of the plasma device.

Couching the perspective by our own efforts concerning the calculation of electron emission yields, the selfconsistent description of electric double layers, and the infrared diagnostics of the wall charge, we bat for an investigation of the plasma-solid interface's electronic structure by in-operando techniques of surface physics. As exemplified by a discussion of dielectric materials, important parameters of the interface's electronic structure are likely to

change in the course of plasma exposure. In particular, information about energy barriers, band bendings, and the presence or absence of surface states has to be obtained in-operando, that is, in experimental settings, where the plasma is on. The most powerful techniques for this purpose are infrared reflection, photoemission, and electron energy loss spectroscopy. However, due to the plasma, they cannot be applied directly to the interface of interest. Alternative setups need to be developed. A possibility for infrared spectroscopy is a setup which uses the solid as an internal reflection element. Photoemission and electron energy loss spectroscopy can be applied in a spinning wall or a from-the-back geometry.

The experiments are challenging but within reach of modern instrumentation. They would provide a wealth of information from which essentially all of present day plasma technology would benefit. Most importantly, however, it would guide the development of a selfconsistent theory of the interface's electronics, including the build-up of the wall charge. Having such a theory at hand, it would be possible to search for ways to manipulate the fate of electrons crossing the interface in either way. Since the operation modii and the surface chemistry of solid-bound gas discharges depend on it, it is thus conceivable that the efforts we hope to initiate by this perspective will in the long run culminate in gas discharges with new functionalities.

ACKNOWLEDGMENTS

It is a pleasure to thank Profs. M. Bauer, M. Bonitz, and K. Rossnagel from the University Kiel, Prof. J. Meichsner from the University Greifswald, and Dr. J. P. van Helden from the INP Greifswald for valuable discussions. Support from the Deutsche Forschungsgemeinschaft through Project No. BR-1994/3-1 is also greatly acknowledged.

AVAILABILITY STATEMENT

Data supporting the findings of this study are available from the corresponding author upon reasonable request.

-
- [1] K.-D. Weltmann, J. F. Kolb, M. Holub, D. Uhrlandt, M. Šimek, K. Ostrikov, S. Hamaguchi, U. Cvelbar, M. Černák, B. Locke, A. Fridman, P. Favia, and K. Becker, *Plasma Process Polym.* **16**, e1800118 (2019).
 - [2] I. Adamovich, S. D. Baalrud, A. Bogaerts, P. J. Bruggeman, M. Capelli, V. Colombo, U. Czarnetzki, U. Ebert, J. G. Eden, P. Favia, D. B. Graves, S. Hamaguchi, G. Hieftje, M. Hori, I. D. Kaganovich, U. Kortshagen, M. J. Kushner, N. J. Mason, S. Mazouffre, S. M. Thagard, H.-R. Metelmann, A. Mizuno, E. Moreau, A. B. Murphy, B. Niemira, G. S. Oehrlein, Z. L. Petrovic, L. C. Pitchford, Y.-K. Pu, S. Rauf, O. Sakai, S. Samukawa, S. Starikovskaia, J. Tenneyson, K. Terashima, M. M. Turner, M. C. M. van de Sanden, and A. Vardelle, *J. Phys. D: Appl. Phys.* **50**, 323001 (2017).
 - [3] C. Charles, *Frontiers in Physics* **2**, 00039 (2014).
 - [4] J. K. Sass, *Vacuum* **33**, 741 (1983).

- [5] W. Schmickler, Chem. Rev. **96**, 3177 (1996).
- [6] R. T. Tung, Appl. Phys. Rev. **1**, 011304 (2014).
- [7] A. Klein, J. Am. Ceram. Soc. **99**, 369 (2016).
- [8] J. Mannhart and D. G. Schlom, Science **327**, 1607 (2010).
- [9] M. A. Raadu, Phys. Reports **178**, 25 (1989).
- [10] C. Charles, Plasma Sources Sci. Technol. **16**, R1 (2007).
- [11] I. Langmuir and H. Mott-Smith, Gen. Electr. Rev. **27**, 449 (1924).
- [12] N. Hershkowitz, Phys. Plasma **12**, 055502 (2005).
- [13] S. Robertson, Plasma Phys. Control. Fusion **55**, 093001 (2013).
- [14] L. A. Schwager and C. K. Birdsall, Phys. Fluids B **2**, 1057 (1990).
- [15] R. P. Brinkmann, J. Phys. D: Appl. Phys. **42**, 194009 (2009).
- [16] R. N. Franklin, J. Phys. D: Appl. Phys. **36**, R309 (2003).
- [17] K.-U. Riemann, J. Phys. D: Appl. Phys. **36**, 2811 (2003).
- [18] J. I. F. Palop, J. Ballesteros, M. A. Hernández, and R. M. Crespo, Plasma Sources Sci. Technol. **16**, S76 (2007).
- [19] F. Taccogna, S. Longo, and M. Capitelli, Phys. Plasma **11**, 1220 (2004).
- [20] J. P. Sheehan, N. Hershkowitz, I. D. Kaganovich, H. Wang, Y. Raitses, E. V. Barnat, B. R. Weatherford, and D. Sydorenko, Phys. Rev. Lett. **111**, 075002 (2013).
- [21] M. D. Campanell and M. V. Umansky, Phys. Rev. Lett. **116**, 085003 (2016).
- [22] S. D. Baalrud, B. Scheiner, B. T. Yee, M. M. Hopkins, and E. Barnat, Plasma Sources Sci. Technol. **29**, 053001 (2020).
- [23] E. Kindel and R. Arndt, Beitr. Plasmaphysik **20**, 119 (1980).
- [24] K. Pangal, S. L. Firebaugh, and J. C. Sturm, Appl. Phys. Lett. **69**, 1471 (1996).
- [25] E. Slikboer, P. Viegas, Z. Bonaventura, E. Garcia-Cauarel, A. Sobota, A. Bourdon, and O. Guaitella, Plasma Sources Sci. Technol. **28**, 095016 (2019).
- [26] T. Kawasaki, T. Terashima, Y. Zhu, T. Takada, and T. Maeno, J. Phys. D: Appl. Phys. **27**, 1646 (1994).
- [27] R. Tschiersch, M. Bogaczyk, and H.-E. Wagner, J. Phys. D: Appl. Phys. **47**, 365204 (2014).
- [28] Y. Raitses, D. Staack, M. Keidar, and N. J. Fisch, Phys. Plasma **12**, 057104 (2005).
- [29] Y. P. Raizer, M. N. Shneider, and N. A. Yatsenko, *Radio-frequency capacitive discharges* (CRC Press, Boca Raton, 2019).
- [30] D. A. Mendis, Plasma Sources Sci. Technol. **11**, A219 (2002).
- [31] O. Ishihara, J. Phys. D: Appl. Phys. **40**, R121 (2007).
- [32] U. Kogelschatz, Plasma Chemistry and Plasma Processing **23**, 1 (2003).
- [33] R. Brandenburg, Plasma Sources Sci. Technol. **26**, 053001 (2017).
- [34] F. Massines, P. Segur, N. Gherardi, C. Khamphan, and A. Ricard, Surface and Coatings Technology **174-175**, 8 (2003).
- [35] H.-E. Wagner, Y. V. Yurgelenas, and R. Brandenburg, Plasma Phys. Control. Fusion **47**, B641 (2005).
- [36] S. Nemschokmichal, R. Tschiersch, H. Höft, R. Wild, M. Bogaczyk, M. M. Becker, D. Loffhagen, L. Stollenwerk, M. Kettlitz, R. Brandenburg, and J. Meichsner, Eur. Phys. J. D **72**, 89 (2018).
- [37] F. J. J. Peeters, R. F. Rumphorst, and M. C. M. van de Sanden, Plasma Sources Sci. Technol. **25**, 03LT03 (2016).
- [38] E. C. Neyts, K. Ostrikov, M. K. Sunkara, and A. Bogaerts, Chem. Rev. **115**, 13408 (2015).
- [39] H. Patel, R. K. Sharma, V. Kyriakou, A. Pandiyan, S. Welzel, M. C. M. van de Sanden, and M. N. Tsampas, ACS Energy Lett. **4**, 2091 (2019).
- [40] M. K. Kulsreshath, L. Schwaederle, L. J. Overzet, P. Lefauchaux, J. Ladroue, T. Tillicher, O. Aubry, M. Woytasik, G. Schelcher, and R. Dussart, J. Phys. D: Appl. Phys. **45**, 285202 (2012).
- [41] J. G. Eden, S.-J. Park, J. H. Cho, M. H. Kim, T. J. Houlahan, B. Li, E. S. Kim, T. L. Kim, S. K. Lee, K. S. Kim, J. K. Yoon, S. H. Sung, P. Sun, C. M. Herring, and C. J. Wagner, IEEE Trans. Plasma Sci. **41**, 661 (2013).
- [42] M. Tabib-Azar and P. Pai, Micromachines **8**, 117 (2017).
- [43] R. Michaud, V. Felix, A. Stolz, O. Aubry, P. Lefauchaux, S. Dzikowski, V. S. von der Gathen, L. J. Overzet, and R. Dussart, Plasma Sources Sci. Technol. **27**, 025005 (2018).
- [44] K. Rasek, F. X. Bronold, and H. Fehske, Phys. Rev. E **102**, 023206 (2020).
- [45] S. Arumugam, M. Perumal, K. P. Anjana, S. V. M. Satyanarayana, and S. K. Sinha, Phys. Plasma **27**, 023512 (2020).
- [46] M. Bonitz, A. Filinov, J.-W. Abraham, K. Balzer, H. Kählert, E. Pehlke, F. X. Bronold, M. Pamperin, M. Becker, D. Loffhagen, and H. Fehske, Front. Chem. Sci. Eng. **13**, 201 (2019).
- [47] G.-Y. Sun, Y. Li, S. Zhang, B.-P. Song, H.-B. Mu, B.-H. Guo, A.-B. Sun, and G.-J. Zhang, Plasma Sources Sci. Technol. **28**, 055001 (2019).
- [48] F. X. Bronold and H. Fehske, J. Phys. D: Appl. Phys. **50**, 294003 (2017).
- [49] L. J. Brillson, *Surfaces and interfaces of electronic materials* (Wiley-VCH Verlag, Weinheim, 2010).
- [50] Y. Liu, Q. Sun, J. Liu, M. N. Banis, Y. Zhao, B. Wang, K. Adair, Y. Hu, Q. Xiao, C. Zhang, L. Zhang, S. Lu, H. Huang, X. Song, and X. Sun, ACS Appl. Mater. Interfaces **12**, 2293 (2020).
- [51] R. Hausbrand, M. Fingerle, T. Späth, and C. Guhl, Thin Solid Films **643**, 43 (2017).
- [52] M. Schnippering, S. R. T. Neil, S. R. Mackenzie, and P. R. Unwin, Chem. Soc. Rev. **40**, 207 (2011).
- [53] E. E. Barritt, C. I. Smith, D. S. Martin, K. Gentz, K. Wandelt, and P. Weightman, Europhys. Lett. **92**, 57005 (2010).
- [54] P. Lange, V. Glaw, H. Neff, E. Piltz, and J. K. Sass, Vacuum **33**, 763 (1983).
- [55] M. V. Varsha and G. Nageswaran, Frontiers in Chemistry **8**, 23 (2020).
- [56] C. Zborowski, O. Renault, A. Torres, C. Guedj, Y. Yamashita, S. Ueda, and G. Grenet, J. Appl. Phys. **124**, 085115 (2018).
- [57] F. J. J. Peeters, J. Zheng, I. M. P. Aarts, A. C. R. Pipino, W. M. M. Kessels, and M. C. M. van de Sanden, J. Vac. Sci. Technol. A **35**, 05C307 (2017).
- [58] A. Tselev, J. Velmurugan, A. V. Ievlev, and S. V. Kalinin, ACS Nano **10**, 3562 (2016).
- [59] M. Copuroglu, H. Sezen, R. L. Opila, and S. Suzer, ACS Appl. Mater. Interfaces **5**, 5875 (2013).

- [60] J. Rubio-Zuazo and G. R. Castro, *Surf. Interface Anal.* **40**, 1438 (2008).
- [61] I. M. P. Aarts, A. C. R. Pipino, M. C. M. van de Sanden, and W. M. M. Kessels, *Appl. Phys. Lett.* **90**, 161918 (2007).
- [62] I. M. P. Aarts, A. C. R. Pipino, J. P. M. Hoefnagels, W. M. M. Kessels, and M. C. M. van de Sanden, *Phys. Rev. Lett.* **95**, 166104 (2005).
- [63] A. Tselev, J. Fagan, and A. Kolmakov, *Appl. Phys. Lett.* **113**, 263101 (2018).
- [64] R. Laha, A. Manivannan, and S. Kasiviswanathan, *Rev. Sci. Instrum.* **85**, 035001 (2014).
- [65] K. Tai, T. J. Houllahan, J. G. Eden, and S. J. Dillon, *Sci. Reports* **3**, 1325 (2013).
- [66] J. Guha, Y.-K. Pu, and V. M. Donnelly, *J. Vac. Sci. Technol. A* **25**, 347 (2007).
- [67] M. Nitschke and J. Meichsner, *J. Appl. Polymer Science* **65**, 381 (1997).
- [68] P. Tolias, *Plasma Phys. Control. Fusion* **56**, 123002 (2014).
- [69] P. Tolias, *Plasma Phys. Control. Fusion* **56**, 045003 (2014).
- [70] J. Marbach, F. X. Bronold, and H. Fehske, *Eur. Phys. J. D* **66**, 106 (2012).
- [71] M. Pamperin, F. X. Bronold, and H. Fehske, *Plasma Sources Sci. Technol.* **27**, 084003 (2018).
- [72] F. X. Bronold and H. Fehske, *Phys. Rev. Lett.* **115**, 225001 (2015).
- [73] F. X. Bronold and H. Fehske, *Plasma Phys. Control. Fusion* **59**, 014011 (2017).
- [74] L. A. Gonzalez, M. Angelucci, R. Larciprete, and R. Cimino, *AIP Advances* **7**, 115203 (2017).
- [75] J. Pierron, C. Inguibert, M. Belhaj, T. Gineste, J. Puech, and M. Raine, *J. Appl. Phys.* **121**, 215107 (2017).
- [76] C. Corbella, A. Marcak, T. de los Arcos, and A. von Keudell, *J. Phys. D: Appl. Phys.* **49**, 16LT01 (2016).
- [77] A. Marcak, C. Corbella, T. de los Arcos, and A. von Keudell, *Rev. Sci. Instrum.* **86**, 106102 (2015).
- [78] A. Dunaevsky, Y. Raitses, and N. J. Fisch, *Phys. Plasma* **10**, 2574 (2003).
- [79] V. A. Zobnin, A. D. Usachev, O. F. Petrov, V. E. Fortov, M. H. Thoma, and M. A. Fink, *Phys. Plasma* **25**, 033702 (2018).
- [80] V. I. Demidov, S. F. Adams, I. D. Kaganovich, M. E. Koepke, and I. P. Kurlyandskaya, *Phys. Plasma* **22**, 104501 (2015).
- [81] M. Daksha, B. Berger, E. Schuengel, I. Korolov, A. Derzsi, M. Koepke, Z. Donkó, and J. Schulze, *J. Phys. D: Appl. Phys.* **49**, 234001 (2016).
- [82] M. Daksha, A. Derzsi, Z. Mujahid, D. Schulenberg, B. Berger, Z. Donkó, and J. Schulze, *Plasma Sources Sci. Technol.* **28**, 034002 (2019).
- [83] J. W. Rabalais, ed., *Low energy ion-surface interaction* (Wiley and Sons, New York, 1994).
- [84] R. C. Monreal, *Progr. Surface Science* **89**, 80 (2014).
- [85] R. Dashen, *Phys. Rev.* **134**, A1025 (1964).
- [86] M. Vicane, *Surf. Sci.* **440**, 1 (1999).
- [87] L. G. Glazov and I. Pázsit, *Nucl. Instr. and Meth. B* **256**, 638 (2007).
- [88] M. P. Seah and W. A. Dench, *Surf. Interf. Anal.* **1**, 2 (1979).
- [89] W. A. Harrison, *Solid state theory* (Dover Publications Inc., New York, 1979).
- [90] Z. Lin, L. V. Zhigilei, and V. Celli, *Phys. Rev. B* **77**, 075133 (2008).
- [91] A. A. Grinberg and S. Luryi, *Solid-St. Electron.* **35**, 1299 (1992).
- [92] A. R. St. Denis and D. L. Pulfrey, *J. Appl. Phys.* **84**, 4959 (1998).
- [93] K. Konistis and Q. Hu, *J. Appl. Phys.* **91**, 5400 (2002).
- [94] M. Li, C. Li, H. Zhan, and J. Xu, *Appl. Phys. Lett.* **92**, 031503 (2008).
- [95] P. F. Ambrico, M. Ambrico, L. Schiavulli, and S. D. Benedictis, *J. Phys. D: Appl. Phys.* **47**, 305201 (2014).
- [96] P. F. Ambrico, M. Ambrico, L. Schiavulli, T. Ligonzo, and V. Augelli, *Appl. Phys. Lett.* **94**, 051501 (2009).
- [97] K. Rasek, F. X. Bronold, M. Bauer, and H. Fehske, *Europhys. Lett.* **124**, 25001 (2018).
- [98] E. Thiessen, F. X. Bronold, and H. Fehske, *Plasma Sources Sci. Technol.* **28**, 095024 (2019).
- [99] K. Kempa and R. R. Gerhardts, *Surf. Sci.* **150**, 157 (1985).
- [100] M. Milosevic, *Internal reflection and ATR spectroscopy* (Wiley, New York, 2012).
- [101] L. Ling, S. Kuwabara, T. Abe, and F. Shimura, *J. Appl. Phys.* **73**, 3018 (1993).
- [102] A. O'Keefe and D. A. G. Deacon, *Rev. Sci. Instrum.* **59**, 2544 (1988).
- [103] F. Bechstedt, *Principles of surface physics* (Springer Verlag, Berlin, 2003).
- [104] R. L. Heinisch, F. X. Bronold, and H. Fehske, *Phys. Rev. B* **83**, 195407 (2011).
- [105] R. L. Heinisch, F. X. Bronold, and H. Fehske, *Phys. Rev. B* **85**, 075323 (2012).
- [106] M. W. Cole, *Rev. Mod. Phys.* **46**, 451 (1974).
- [107] M. J. Rutter and J. Robertson, *Phys. Rev. B* **57**, 9241 (1998).
- [108] J. B. Cui, J. Ristein, and L. Ley, *Phys. Rev. Lett.* **81**, 429 (1998).
- [109] H. Yamaguchi, T. Masuzawa, S. Nozue, Y. Kudo, I. Saito, J. Koe, M. Kudo, T. Yamada, Y. Takakuwa, and K. Okano, *Phys. Rev. B* **80**, 165321 (2009).
- [110] K. P. Loh, I. Sakaguchi, M. N. Gamo, S. Tagawa, T. Sugino, and T. Ando, *Appl. Phys. Lett.* **74**, 28 (1999).
- [111] M. Rohlfing, N.-P. Wang, P. Krueger, and J. Pollmann, *Phys. Rev. Lett.* **91**, 256802 (2003).
- [112] K. P. McKenna and A. L. Shluger, *Nature Materials* **7**, 859 (2008).
- [113] Y. R. Wang and C. B. Duke, *Surf. Sci.* **192**, 309 (1987).
- [114] A. R. McNeill, A. R. Hyndman, R. J. Reeves, and A. J. Downard, *ACS Appl. Mater. Interf.* **8**, 31392 (2016).
- [115] F. Maier, J. Ristein, and L. Ley, *Phys. Rev. B* **64**, 165411 (2001).
- [116] K. J. Rietwyk, S. L. Wong, L. Cao, K. M. O'Donnell, L. Ley, and A. T. S. Wee, *Appl. Phys. Lett.* **102**, 091604 (2013).
- [117] J. M. A. Beattie, J. P. Gross, M. J. Rayson, and P. R. Briddon, *Diamond and Related Materials* **94**, 137 (2019).
- [118] T. C. Rödel, F. Fortuna, F. Bertran, M. Gabay, M. J. Rozenberg, A. F. Santander-Syro and P. Le Fèvre, *Phys. Rev. B* **92**, 041106 (2015).
- [119] W.-J. Yin, B. Wen, C. Zhou, A. Selloni, and L.-M. Liu, *Surf. Sci. Rep.* **73**, 58 (2018).
- [120] H. Ade, W. Yang, S. L. English, J. Hartman, R. F. Davies, R. J. Nemanich, V. N. Litvinenko, I. V. Pinayev,

- Y. Wu, and J. M. J. Madey, Surf. Rev. Lett. **5**, 1257 (1998).
- [121] I. Mahboob, T. D. Veal, C. F. McConville, H. Lu, and W. J. Schaff, Phys. Rev. Lett. **92**, 036804 (2004).
- [122] Y. Dou, R. G. Egdell, T. Walker, D. S. L. Law, and G. Beamson, Surf. Sci. **398**, 241 (1998).
- [123] H. Lüth, Vacuum **38**, 223 (1988).
- [124] H. Ibach and D. L. Mills, *Electron energy loss spectroscopy and surface vibrations* (Academic Press, New York, 1982).